Published in final edited form as:
Biochemistry. 2009 October 13; 48(40): 9641–9649. doi:10.1021/bi900879a.

Reaction Mechanism of *cis*-3-Chloroacrylic Acid Dehalogenase - A Theoretical Study‡

Robin Sevastik[§], **Christian P. Whitman**[$,*], and **Fahmi Himo**[§,*]

[§]Department of Organic Chemistry, Arrhenius Laboratory, Stockholm University, SE-106 91 Stockholm, Sweden

[$]Division of Medicinal Chemistry, College of Pharmacy, University of Texas at Austin, Austin, TX 78712, USA

Abstract

The reaction mechanism of *cis*-3-chloroacrylic acid dehalogenase (*cis*-CaaD) is studied using the density functional theory method B3LYP. This enzyme catalyzes the hydrolytic dehalogenation of *cis*-3-chloroacrylic acid to yield malonate semialdehyde and HCl. The uncatalyzed reaction is first considered and excellent agreement is found between the calculated barrier and the measured rate constant. The enzymatic reaction is then studied with an active site model consisting of 159 atoms. The results suggest an alternative mechanism for *cis*-CaaD catalysis and different roles for some active site residues in this mechanism.

cis-3-Chloroacrylic acid dehalogenase (*cis*-CaaD) is a bacterial enzyme that catalyzes the hydrolytic dehalogenation of *cis*-3-chloroacrylic acid to produce malonate semialdehyde and HCl [1–3]. *cis*-CaaD is part of a degradation pathway in the soil bacterium *Pseudomonas pavonaceae* allowing the bacteria to utilize 1,3-dichloropropene, a pesticide that is degraded to *cis*-3-chloroacrylic acid, as a source of carbon and energy [4].

cis-CaaD is a trimer composed of three identical monomers with 149 amino acids per monomer [5]. It belongs to the tautomerase superfamily and shares sequence similarity with 4-oxalocrotonate tautomerase (4-OT) and *trans*-3-chloroacrylic acid dehalogenase (CaaD) [6–7]. The latter enzyme catalyzes the same reaction as *cis*-CaaD but utilizes the *trans*-substrate. All of the enzymes characterized thus far in the tautomerase superfamily have a catalytic terminal proline residue (Pro-1). In 4-OT, Pro-1 has a pK_a value of ~6.4 and is proposed to act as a base, abstracting a proton from the substrate [8]. In *cis*-CaaD, Pro-1 could act as a catalytic base to activate a water molecule for attack, or it could function as a catalytic acid and provide a proton at C2 of substrate to complete the conjugate addition of water. The pK_a of Pro-1 in CaaD has been determined to ~9.2 by direct NMR titration [9]. In *cis*-CaaD a direct NMR titration has not been performed. However, a pH rate profile implicates a group in catalysis in the free enzyme with a pK_a of ~9.3 [10]. These results point towards Pro-1 being cationic in *cis*-CaaD, suggesting Pro-1 is not a catalytic base, but an acid.

All three enzymes have at least two arginine groups in the active site (Arg-70 and Arg-73 in *cis*-CaaD) that interact with the substrate's C1 carboxylate group. In *cis*-CaaD the roles of the arginine groups could be to draw electron density away from C3, facilitating the addition of water. Both CaaD and *cis*-CaaD have a glutamate residue in the active site (Glu-114 in *cis*-

This work was supported by: The Swedish Research Council (FH) and the National Institutes of Health Grant GM-65324 (CPW).

*To whom correspondence should be addressed: CPW: Tel: +1-512-471-6198. Fax: +1-512-232-2606. whitman@mail.utexas.edu; FH: Tel: +46-8-161094. Fax: +46-8-154908. himo@organ.su.se.

CaaD), which could be a potential base for activating the water molecule. An additional residue, His-28, is located near the two arginines in *cis*-CaaD. His-28 may assist in positioning the substrate and/or polarizing it via an interaction with the C-1 carboxylate group.

Based on experimental studies [11–13] a general mechanism for the *cis*-CaaD reaction has been proposed (Scheme 2). A base (i.e., Glu-114) in the active site activates a water molecule for attack at the C3 position of substrate to form a tetrahedral intermediate. The tetrahedral intermediate then collapses to an enol intermediate (path a), which is followed by ketonization to give the final product. Alternatively, the tetrahedral intermediate picks up a proton at C-2 (path b) followed by collapse and release of HCl and product.

The barriers for the uncatalyzed and the CaaD-catalyzed reaction of the dehalogenation of *trans*-3-chloroacrylic acid have been determined experimentally to be ~33.3 kcal/mol and 16.6 respectively [14]. *trans*-CaaD thereby achieves a $\sim 10^{12}$ fold rate enhancement. A similar rate enhancement for *cis*-CaaD can be assumed in view of the similarities between the two substrates and enzymes.

In the present study, we investigate the reaction mechanism of *cis*-CaaD using the B3LYP density functional theory method [15–18]. A relatively large model of the active site (159 atoms) is constructed and the two different mechanistic hypotheses are considered (Scheme 2). In addition, the impact of the protonation state of Pro-1 is considered on the mechanism. This approach has been proven very useful in the study of a wide variety of enzymatic reactions [19–33]. In particular, we have previously used the same approach to investigate the reaction mechanism of 4-oxalocrotonate tautomerase [28].

II. Computational Details

All geometries and energies presented in this study are computed using the B3LYP [15–18] density functional theory method as implemented in the Gaussian03 program package [34]. Geometry optimizations were performed using the 6-31G(d,p) basis set. Based on these geometries, single point calculations with the larger basis set 6-311+G(2d,2p) were done to obtain more accurate energies. Solvation energies were added as single point calculations using the conductor-like solvation model CPCM [35–36] at the B3LYP/6-31G(d,p) level. In this model, a cavity around the system is surrounded by a polarizable dielectric continuum. For the uncatalyzed solution reaction (see Section IIIa below), a dielectric constant of 80 is used to model the water surrounding. To model the enzyme surrounding, ε=4 is used. However, since this value is rather arbitrary, the results using ε=80 are also reported here in order to give an idea about the sensitivity of the results. In the active site model, some centers were kept fixed to their X-ray positions in the geometry optimization. The size of the model (i.e., 159 atoms) prohibited the calculation of frequencies and thus the determination of the zero-point vibrational energies and the entropy effects. The energies reported here correspond thus to enthalpies. Another problem related to the size of the model is the multiple-minima problem. To avoid that the stationary points lie in different local minima, which can lead to unreliable relative energies, we have by careful visual inspection done our best to confirm that the parts that do not directly participate in the reaction are in the same local minima throughout the reaction.

III. Results and Discussion

IIIa. Model of Uncatalyzed Reaction

Wolfenden and co-workers measured the uncatalyzed rate for the hydrolytic dehalogenation of the *trans*-isomer to be 2.2×10^{-12} s^{-1}, which corresponds to a rate-limiting barrier of 33.3 kcal/mol [14]. The uncatalyzed rate for the *cis*-isomer is likely to be comparable. We devised

a small model consisting of the *cis*-3-chloroacrylic acid substrate and two water molecules to study the uncatalyzed reaction. The optimized stationary points are shown in Figure 1, and the calculated energies are displayed in Figure 2.

In the first step, one water molecule attacks at the C-3 carbon, while the second water shuttles the proton from the nucleophilic water to the carboxylate moiety of the substrate. At the transition state, the critical O–C distance is 2.05 Å, and the C–Cl distance is 1.81 Å (only slightly longer than the 1.77 Å calculated for the reactant species). It turns out that the nucleophilic attack and the displacement of the chloride ion take place in a single step. Numerous attempts were made to locate a tetrahedral intermediate (e.g., **1** in Scheme 2) without success. The barrier is calculated to be 30.2 kcal/mol and the reaction step was found to be exothermic by as much as 27.3 kcal/mol. Addition of solvation in the form of polarizable continuum model (PCM) with a dielectric constant of ε=80 had very little effect on these energies (Figure 2). The barrier increased slightly to 31.8 kcal/mol and the reaction energy was slightly raised, to −25.7 kcal/mol. The calculated barrier agrees very well with the experimental value of 33.3 kcal/mol. This indicates that the model, despite its small size, captures the important features of the reaction.

The second step is a 1,3-keto-enol tautomerization step to give malonate semialdehyde. This step was also studied with help of two water molecules (**4**, Figure 1). In gas phase, this reaction step is slightly exothermic (−1.4 kcal/mol), while upon addition of solvation (ε=80), it is slightly endothermic (+1.9 kcal/mol). We have located the transition state (**5**, Figure 1) and the barrier was calculated to be 16.8 kcal/mol. When solvation was added, the barrier became 19.9 kcal/mol.

The addition of more water molecules to the model did not change the energies significantly. For example, the barrier for the first step was calculated to be 34.0 (ε=80) kcal/mol when using five water molecules in the model.

Two conclusions can be drawn from the results of our study of the non-enzymatic reaction. First, the rate-limiting barrier for the transformation is found for the first step, which is a nucleophilic attack and chloride release. The enzymatic barrier has been estimated to 16.6 kcal/mol [14], which means that *cis*-CaaD has to lower the barrier of the first step by more than 16 kcal/mol, assuming it uses a similar reaction mechanism. The second conclusion is that since the barrier of the second step is relatively low, it is possible that this step could be non-enzymatic, taking place outside the enzyme. This suggests that *cis*-CaaD may only catalyze the first step of the reaction.

IIIb. Model of Enzymatic Reaction

A model of the *cis*-CaaD active site was built based on the native crystal structure (PDB code 2FLZ [5]). The model consists of parts of the following residues (as shown schematically in Figure 3): Pro-1, Glu-114, Tyr-103', Leu-119, Arg-70, His-69, Arg-73, His-28, and Thr-34 (where the prime indicates that the residue comes from an adjacent monomer). The substrate was not present in the native crystal structure and had therefore to be superimposed based on the crystal structure of *cis*-CaaD inactivated by (*R*)-oxirane-2-carboxylate (PDB code 2FLT). Inactivation results from the covalent attachment of (*R*)-2-hydroxypropanoate on Pro-1 [5]. Also, the water molecule was added manually in the vicinity of the potential bases Pro-1 and Glu-114. The model consists thus of 159 atoms and the total charge is 0. To maintain the overall active site structure and to avoid artificial movements of various groups, certain atoms were locked in their crystallographic positions. These are typically the positions where the truncation is made. These positions are indicated by stars in the figures below.

In the optimized reactant structure, the two arginines (Arg-70 and Arg-73) and the histidine (His-28) bind the carboxylate moiety of the substrate, thereby positioning it in the active site. The water molecule is in good position to attack C-3 of substrate, with an O−C3 distance of 3.66 Å. The water is hydrogen-bonded to Pro-1 (2.43 Å) and Glu-114 (2.32 Å), indicating that both of these groups are possible bases that can activate the water. It should be noted that the optimal pH for the reaction is ~9.0 [8]. If the pK_a of Pro-1 is ~9.2, then a significant percentage of the enzyme has a neutral Pro-1 (~40%) and a cationic Pro-1 (~60%).

We optimized the transition state for the nucleophilic attack of water (Figure 3C). As in the case of the uncatalyzed reaction, this step turns out to be coupled to the release of the chloride ion. At the TS, the O−C3 distance is 1.76 Å and the C3-Cl distance increased from 1.75 Å in the reactant to 1.80 Å. The water hydrogen bonds to Pro-1 and Glu-114 are also significantly shorter, 1.62 Å and 1.60 Å, respectively.

In the resulting enol intermediate, the chloride is totally released. It turns out that the proton of the water is transferred to Pro-1, which in turn transferred its proton to Glu-114. Glu-114 is thus the catalytic base that activates the water molecule and one of the functions of Pro-1 could be to shuttle the proton.

The calculated barrier for this step is 22.3 kcal/mol, which upon inclusion of solvation effects decreases slightly to 21.9 and 21.7 kcal/mol, using dielectric constants of ε = 4 and ε = 80, respectively. As in the non-enzymatic case, the reaction step is highly exothermic, by 33.6, 36.9, and 38.3 kcal/mol, without solvation and with solvation using ε = 4 and ε = 80, respectively.

In this kind of dehalogenation reactions where an ion is released in the active site, the electrostatic interactions with the enzyme surrounding are expected to contribute significantly to the energetics. However, the fact that the solvation effects are quite small (less than one kcal/mol for the barrier) indicates that the chosen model is adequate for describing this kind of reactions. This is an important result that is in line with previous experience from enzyme modeling where we have observed that the solvation effects saturate at a model size similar to the one used in this study [28,32].

Once the enol intermediate has formed in the *cis*-CaaD enzyme a ketonization reaction follows to generate the final product. This could take place outside the enzyme. The barrier for this is calculated to be 19.9 kcal/mol, as discussed above.

To model the tautomerization step at the active site, we removed the chloride ion from the model and reoptimized the enol intermediate (Figure 4A). We note that there exists a hydrogen bonding network that connects the substrate enol to Pro-1, which is in perfect position to protonate the C2 carbon of the substrate. This network involves the Tyr-103’ and Glu-114 residues.

We tried to locate a transition state in which the proton is transferred concertedly through this chain, but without success. Instead, the enzymatic tautomerization was found to proceed in a stepwise fashion. First, a proton was transferred from Glu-114 to Pro-1. This step has a very small barrier of 0.6 kcal/mol and is slightly exothermic (by 2.2 kcal/mol, values referring to ε=4). Next, a concerted proton transfer from the substrate enol to Tyr-103’ coupled with a proton transfer from Tyr-103’ to Glu-114 takes place. The barrier for this step is also quite low (6.2 kcal/mol) and it is slightly endothermic (+2.0 kcal/mol). Finally, the cationic Pro-1 can now deliver the proton to the C2 position of the substrate, thereby completing the reaction. This step has a significant barrier of 13.6 kcal/mol, which, when added to the endothermicity of the previous step, becomes 15.6 kcal/mol. The overall enzymatic ketonization reaction is

thus endothermic by 8.2 kcal/mol. The optimized structures are shown in Figure 4 and the calculated energies of the entire *cis*-CaaD reaction are summarized in Figure 5.

Hence, according to this model, the difference between the enzymatic and non-enzymatic keto-enol tautomerization step is quite small (ca 4 kcal/mol) and within the error margin, which leaves it possible that the reaction takes place outside the active site.

IIIc. Alternative water binding

Since it is unknown how the substrate and the water molecule bind relative to each other in the active site, we examined an alternative binding mode in which the water is positioned on the other face of the substrate, i.e., far from Pro-1 (see Figure 6). The water now forms a hydrogen bond to the Tyr-103' residue instead of the Pro-1 and Glu-114 in the former case (see above).

Also for this model, we optimized the transition state for nucleophilic attack of water and found that attack and release of the chloride ion occur in a single step. The catalytic base is the same, Glu-114. However, Tyr-103' takes the role of the Pro-1 residue in shuttling the proton to the base.

The calculated barrier for this scenario is 20.6 kcal/mol, which upon inclusion of salvation increases to 26.4 and 28.5 kcal/mol using $\varepsilon = 4$ and $\varepsilon = 80$, respectively. These values are significantly higher than those calculated for the other binding mode, making this scenario less likely.

IIId. Cationic Pro-1

In the calculations presented above, Pro-1 was modeled in the neutral form. However, as noted above, a significant fraction (~60%) is cationic and it has been proposed that Pro-1 functions as a general acid [9]. Therefore, we constructed a model of the active site where Pro-1 was in the cationic form. The model has a total of 160 atoms and a total charge of +1 (Figure 7).

In the reactant structure the water is in a good position to attack the substrate, with an O-C3 distance of 3.56 Å, and the water is hydrogen bonded to the Glu-114 residue.

For this model we have optimized the transition state for the nucleophilic attack, which is coupled with the dehalogenation of the substrate. In this model, Glu-114 acts directly as the catalytic base, activating the nucleophilic water molecule. In the transition state, the critical O-C3 distance is 1.77Å and the C3-Cl distance is 1.81 Å.

The calculated barrier is 27.6 kcal/mol, which increases to 31.7 and 33.1 kcal/mol when using ε=4 and ε=80, respectively. These values are about 10 kcal/mol higher than the one calculated for the neutral proline case, arguing strongly against a cationic Pro-1.

One striking result here is the reaction energy of this step. With a neutral proline, the reaction step is highly exothermic (36.9 kcal/mol using ε=4). However, with a cationic proline, this value is only −3.2 kcal/mol, despite the fact that the catalytic base is the same Glu-114. This can be understood if one considers the Glu-Pro dyad as one unit. This unit is negatively-charged when Pro-1 is neutral (Glu-COO^- −Pro-NH), and neutral when Pro-1 is cationic (Glu-COO^- −Pro-NH_2^+ or alternatively Glu-COOH−Pro-NH). Thus, the proton affinity of this Glu-Pro unit is considerably different in the two cases. In the latter case, the Glu-Pro unit is a worse proton acceptor and thus a worse base, which explains the large difference in the calculated exothermicities.

IIIe. Mechanistic Implications

In the current working hypothesis for the *cis*-CaaD mechanism, Tyr-103 and Glu-114 work together (in some fashion) to activate a water molecule for attack at C-3 of the substrate [2,[5], 10]. In this scenario, His-28 and the pair of arginine residues (Arg-70 and Arg-73) bind and activate the substrate via the C-1 carboxylate group. This interaction polarizes the substrate such that a partial positive charge develops at C-3, which facilitates the attack of water at C-3. Pro-1, functioning as a catalytic acid, adds a proton to C-2 to complete the addition of water. The finding that the reaction is more energetically favorable when a neutral proline is involved (rather than a cationic proline) is obviously at odds with the currently proposed mechanism, particularly with the roles of Pro-1, Tyr-103, and Glu-114.

The *cis*-CaaD mechanism was formulated based on sequence similarities and mechanistic parallels with CaaD, coupled with crystallographic observations of the unliganded *cis*-CaaD enzyme and the enzyme inactivated by (*R*)-oxirane-2-carboxylate [2,[5],10]. A sequence alignment with CaaD first identified the common four groups (i.e., Pro-1, Arg-70, Arg-73, and Glu-114) [2]. Mutagenesis analysis confirmed the importance of these groups, but suggested a subtle mechanistic difference: the Gln-114 mutant retained a significant amount of activity whereas the α-Gln-52 mutant of CaaD had no activity. The crystallographic observations identified two more residues (His-28 and Tyr-103) and pointed to a more complex mechanism for *cis*-CaaD [5]. A very recent pre-steady state kinetic analysis of the *cis*-CaaD reaction suggested that a short loop closes down on the active site upon substrate binding (B.A. Robertson, G. K. Schroeder, Z. Jin, K. A. Johnson, and C.P. Whitman, 2009, unpublished results). The loop is not present in CaaD, indicating yet another mechanistic difference. Thus, as new details emerge about the *cis*-CaaD mechanism, it is becoming apparent that there may only be limited parallels between CaaD and *cis*-CaaD and some of the underlying assumptions used to formulate the *cis*-CaaD mechanism may not be entirely valid. One assumption concerns the protonation state of the prolyl nitrogen in *cis*-CaaD. The pK_a of the prolyl nitrogen (βPro-1) in CaaD has been determined to be 9.2 by direct titration using ^{15}N NMR spectroscopy [9]. A direct titration of the Pro-1 in *cis*-CaaD has not been carried out, but a pH rate profile of the *cis*-CaaD reaction implicated an acid catalyst with a pK_a of 9.3 in the reaction [12]. It is assumed that this pK_a value corresponds to that of Pro-1 (and that the acid catalyst is Pro-1) based on the coincident pK_a values and the mechanistic parallels.

The results of the present study suggest that this assumption and the role of Pro-1 in the reaction should be examined in more detail.

A second assumption concerns the roles of Tyr-103 and Glu-114. The assigned roles for these residues are based on their positions in the crystal structures of the native and inactivated enzyme complex (along with the analogous role of αGlu-52 in CaaD). It may be that the interactions of these two residues and their possible interactions with Pro-1 may be more complex. One possible mechanism is shown in Scheme 3.

IV. Conclusions

In the present study, we investigated the reaction mechanism of *cis*-CaaD using density functional theory calculations and a large active site model.

First, a model of the uncatalyzed reaction was studied and excellent agreement was found with the experimental rate. The calculations indicate that the nucleophilic attack of water at the C-2 carbon and release of the chloride ion happen in one step.

The enzymatic reaction mechanism suggested from the calculations is summarized in Scheme 3. Similar to the water reaction, the enzymatic nucleophilic attack and dehalogenation step are

calculated to happen in one step. Glu-114 acts as the catalytic base to activate the nucleophilic water molecule. However, Pro-1 might shuttle the proton from water to the base. Mutagenic analysis shows that replacement of Pro-1 with an alanine reduced activity to an undetectable rate, whereas changing Glu-114 to a glutamine decreased activity by only 6-8-fold (as assessed by k_{cat}/K_m) [2]. These results are consistent with the calculated mechanism since it is conceivable that removal of the proline shuttle makes it more difficult to activate the water, while when the Glu-114 base is removed, Pro-1 itself can act as the catalytic base in an analogous fashion to its function in the related enzyme 4-oxalocrotonate tautomerase.

Next, a ketonization reaction takes place to complete the reaction. The calculations indicate that it is possible for the active site Tyr-Glu-Pro triad to shuttle the proton from the oxygen to the carbon (in a stepwise fashion). The calculated barrier for this is 15.6 kcal/mol compared to the 19.9 kcal/mol calculated for the non-enzymatic counterpart.

The calculated rate-limiting barrier of ca 22 kcal/mol is somewhat overestimated compared to the experimentally-determined barrier for the closely related *trans*-CaaD (16.6 kcal/mol [14]). Several sources of error are envisioned. As always in quantum chemical studies, the computational method (in this case the DFT/B3LYP functional and the employed basis sets) cannot be ruled out as a possible source of error. Another error could be introduced by the size of the model used in the investigations. Inclusion of more active site groups might lead to a lower reaction barrier. Also, locking truncation atoms can lead to a model that is somewhat rigid, which causes the barriers to be higher. Finally, the crystal structure used for the modeling is that of the irreversibly inactivated enzyme. It is not known how accurately this structure reflects substrate binding and turnover. These inaccuracies coupled with the obtained resolution of the structure can easily translate into errors in the calculations.

In this study we also considered the possibility of the Pro-1 being cationic. However, the barrier was found to be much higher, arguing against this option. Also, an alternative binding mode of the nucleophilic water relative to the substrate was considered, in which the Tyr-103' residue would act as the proton shuttle instead of Pro-1. However, the barrier becomes significantly higher, rendering this possibility less likely. The calculated energies for the various scenarios are summarized in Table 1.

References

1. Poelarends GJ, Saunier R, Janssen DB. *trans*-3-chloroacrylic acid dehalogenase from Pseudomonas pavonaceae 170 shares structural and mechanistic similarities with 4-oxalocrotonate tautomerase. J. Bacteriol 2001;183:4269–4277. [PubMed: 11418568]
2. Poelarends GJ, Serrano H, Person MD, Johnson WH Jr. Murzin AG, Whitman CP. Cloning, expression, and characterization of a *cis*-3-chloroacrylic acid dehalogenase: Insights into the mechanistic, structural, and evolutionary relationship between isomer-specific 3-chloroacrylic acid dehalogenases. Biochemistry 2004;43:759–772. [PubMed: 14730981]
3. Wang SC, Person MD, Johnson WH Jr. Whitman CP. Reactions of *trans*-3-chloroacrylic acid dehalogenase with acetylene substrates: Consequences of and evidence for a hydration reaction. Biochemistry 2003;42:8762–8773. [PubMed: 12873137]
4. Poelarends GJ, Wilkens M, Larkin MJ, van Elsas JD, Janssen DB. Degradation of 1,3-dichloropropene by *Pseudomonas cichorii* 170. Appl. Environ. Microbiol 1998;64:2931–2936. [PubMed: 9687453]
5. de Jong RM, Bazzaco P, Poelarends GJ, Johnson WH Jr. Kim YJ, Burks EA, Serrano H, Thunnissen A-MWH, Whitman CP, Dijkstra BW. Crystal structures of native and inactivated *cis*-3-chloroacrylic acid dehalogenase - Structural basis for substrate specificity and inactivation by (*R*)-oxirane-2-carboxylate. J. Biol. Chem 2007;282:2440–2449. [PubMed: 17121835]
6. Whitman CP. The 4-oxalocrotonate tautomerase family of enzymes: how nature makes new enzymes using a beta-alpha-beta structural motif. Arch. Biochem. Biophys 2002;402:1–13. [PubMed: 12051677]

7. Poelarends GJ, Whitman CP. Evolution of enzymatic activity in the tautomerase superfamily: mechanistic and structural studies of the 1,3-dichloropropene catabolic enzymes. Bioorg. Chem 2004;32:376–392. [PubMed: 15381403]
8. Stivers JT, Abeygunawardana C, Mildvan AS, Hajipour G, Whitman CP. 4-Oxalocrotonate tautomerase: pH dependence of catalysis and p*K*(a) values of active site residues. Biochemistry 1996;35:814–823. [PubMed: 8547261]
9. Azurmendi HF, Wang SC, Massiah MA, Poelarends GJ, Whitman CP, Mildvan AS. The roles of active-site residues in the catalytic mechanism of *trans*-3-chloroacrylic acid dehalogenase: A kinetic, NMR, and mutational analysis. Biochemistry 2004;43:4082–4091. [PubMed: 15065850]
10. Poelerands GJ, Serrano H, Johnson WH Jr. Whitman CP. Stereospecific alkylation of *cis*-3-chloroacrylic acid dehalogenase by (*R*)-oxirane-2-carboxylate: Analysis and mechanistic implications. Biochemistry 2004;43:7187–7196. [PubMed: 15170356]
11. de Jong RM, Brugman W, Poelarends GJ, Whitman CP, Dijkstra BW. The X-ray structure of *trans*-3-chloroacrylic acid dehalogenase reveals a novel hydration mechanism in the tautomerase superfamily. J. Biol. Chem 2004;279:11546–11552. [PubMed: 14701869]
12. Poelarends GJ, Johnson WH Jr. Serrano H, Whitman CP. Phenylpyruvate tautomerase activity of *trans*-3-chloroacrylic acid dehalogenase: Evidence for an enol intermediate in the dehalogenase reaction? Biochemistry 2007;46:9596–9604. [PubMed: 17661448]
13. Poelarends GJ, Almrud JJ, Serrano H, Darty JE, Johnson WH Jr. Hackert ML, Whitman CP. Evolution of enzymatic activity in the tautomerase superfamily: Mechanistic and structural consequences of the L8R mutation in 4-oxalocrotonate Tautomerase. Biochemistry 2006;45:7700–7708. [PubMed: 16784221]
14. Horvat CM, Wolfenden RV. A persistent pesticide residue and the unusual catalytic proficiency of a dehalogenating enzyme. Proc. Natl. Acad. Sci. USA 2005;102:16199–16202. [PubMed: 16260733]
15. Becke AD. Density-functional exchange-energy approximation with correct asymptotic-behavior. Phys. Rev. A 1988;38:3098–3100. [PubMed: 9900728]
16. Becke AD. Density-functional thermochemistry 1. The effect of the exchange-only gradient correction. J. Chem. Phys 1992;96:2155–2160.
17. Becke AD. Density-functional thermochemistry 2. The effect of the Perdew-Wang generalized-gradient correlation correction. J. Chem. Phys 1992;97:9173–9177.
18. Becke AD. Density-functional thermochemistry 3. The role of exact exchange. J. Chem. Phys 1993;98:5648–5652.
19. Himo F, Siegbahn PEM. Quantum chemical studies of radical-containing enzymes. Chem. Rev 2003;103:2421–2456. [PubMed: 12797836]
20. Himo F. Quantum chemical modeling of enzyme active sites and reaction mechanisms. Theor. Chem. Acc 2006;116:232–240.
21. Siegbahn PEM, Himo F. Recent developments of the quantum chemical cluster approach for modeling enzyme reactions. J. Biol. Inorg. Chem 2009;14:643–651. [PubMed: 19437047]
22. Hopmann KH, Hallberg BM, Himo F. Catalytic mechanism of limonene epoxide hydrolase, a theoretical study. J. Am. Chem. Soc 2005;127:14339–14347. [PubMed: 16218628]
23. Velichkova P, Himo F. Methyl transfer in glycine N-methyltransferase. A theoretical study. J. Phys. Chem. B 2005;109:8216–8219. [PubMed: 16851960]
24. Himo F, Guo J-D, Rinaldo-Matthis A, Nordlund P. Reaction mechanism of deoxyribonucleotidase: A theoretical study. J. Phys. Chem. B 2005;109:20004–20008. [PubMed: 16853585]
25. Hopmann KH, Himo F. Theoretical study of the full reaction mechanism of human soluble epoxide hydrolase. Chem. Eur. J 2006;12:6898–6909.
26. Velichkova P, Himo F. Theoretical study of the methyl transfer in guanidinoacetate methyltransferase. J. Phys. Chem. B 2006;110:16–19. [PubMed: 16471489]
27. Chen S-L, Fang W-H, Himo F. Theoretical study of the phosphotriesterase reaction mechanism. J. Phys. Chem. B 2007;111:1253–1255. [PubMed: 17253743]
28. Sevastik R, Himo F. Quantum chemical modeling of enzymatic reactions: The case of 4-oxalocrotonate tautomerase. Bioorg. Chem 2007;35:444–457. [PubMed: 17904194]

29. Chen S-L, Marino T, Fang W-H, Russo N, Himo F. Peptide hydrolysis by the binuclear zinc enzyme aminopeptidase from Aeromonas proteolytica: A density functional theory study. J. Phys. Chem. B 2008;112:2494–2500. [PubMed: 18247603]

30. Liao R-Z, Yu J-G, Raushel FM, Himo F. Theoretical investigation of the reaction mechanism of the dinuclear zinc enzyme dihydroorotase. Chem. Eur. J 2008;14:4287–4292.

31. Hopmann KH, Himo F. Cyanolysis and azidolysis of epoxides by haloalcohol dehalogenase: Theoretical study of the reaction mechanism and origins of regioselectivity. Biochemistry 2008;47:4973–4982. [PubMed: 18393443]

32. Hopmann KH, Himo F. Quantum chemical modeling of the dehalogenation reaction of haloalcohol dehalogenase. J. Chem. Theor. Comp 2008;4:1129–1137.

33. Liao R-Z, Yu J-G, Himo F. Reaction Mechanism of the Dinuclear Zinc Enzyme N-Acyl-L-homoserine Lactone Hydrolase: A Quantum Chemical Study. Inorg. Chem 2009;48:1442–1448.

34. Gaussian 03, Revision C.02. Wallingford CT: Frisch, MJ Gaussian, Inc.; 2004.

35. Barone V, Cossi M. Quantum calculation of molecular energies and energy gradients in solution by a conductor solvent model. J. Phys. Chem. A 1998;102:1995–2001.

36. Cossi M, Rega N, Scalmani G, Barone V. Energies, structures, and electronic properties of molecules in solution with the C-PCM solvation model. J. Comp. Chem 2003;24:669–681. [PubMed: 12666158]

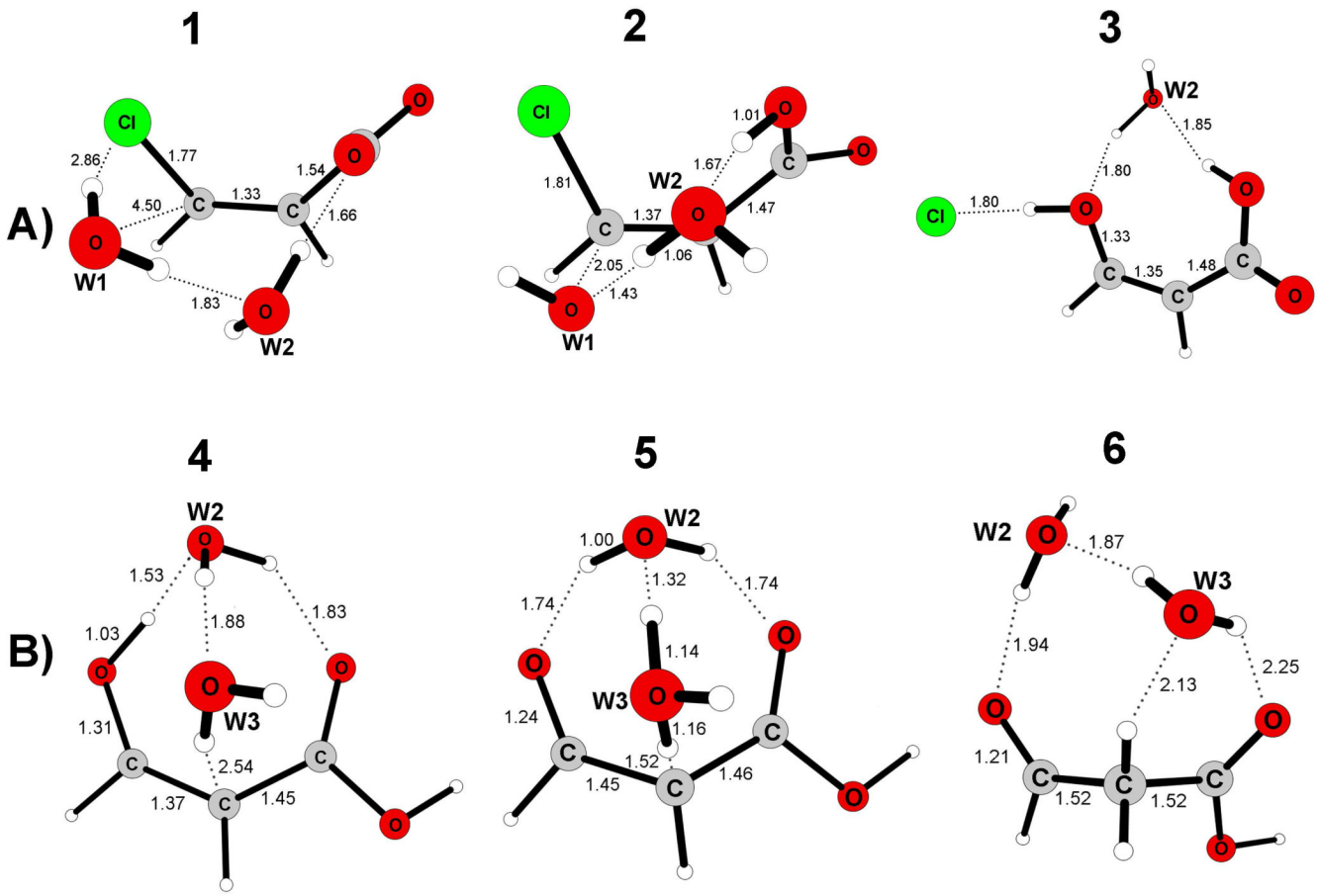

Figure 1.
Optimized stationary points for the first dehalogenation step (A) and the second tautomerization step (B) of the non-enzymatic reaction. 1) Reactant structure, 2) Transition state, 3) Enol-intermediate, 4) Enol-intermediate, 5) Transition state, 6) Keto-product.

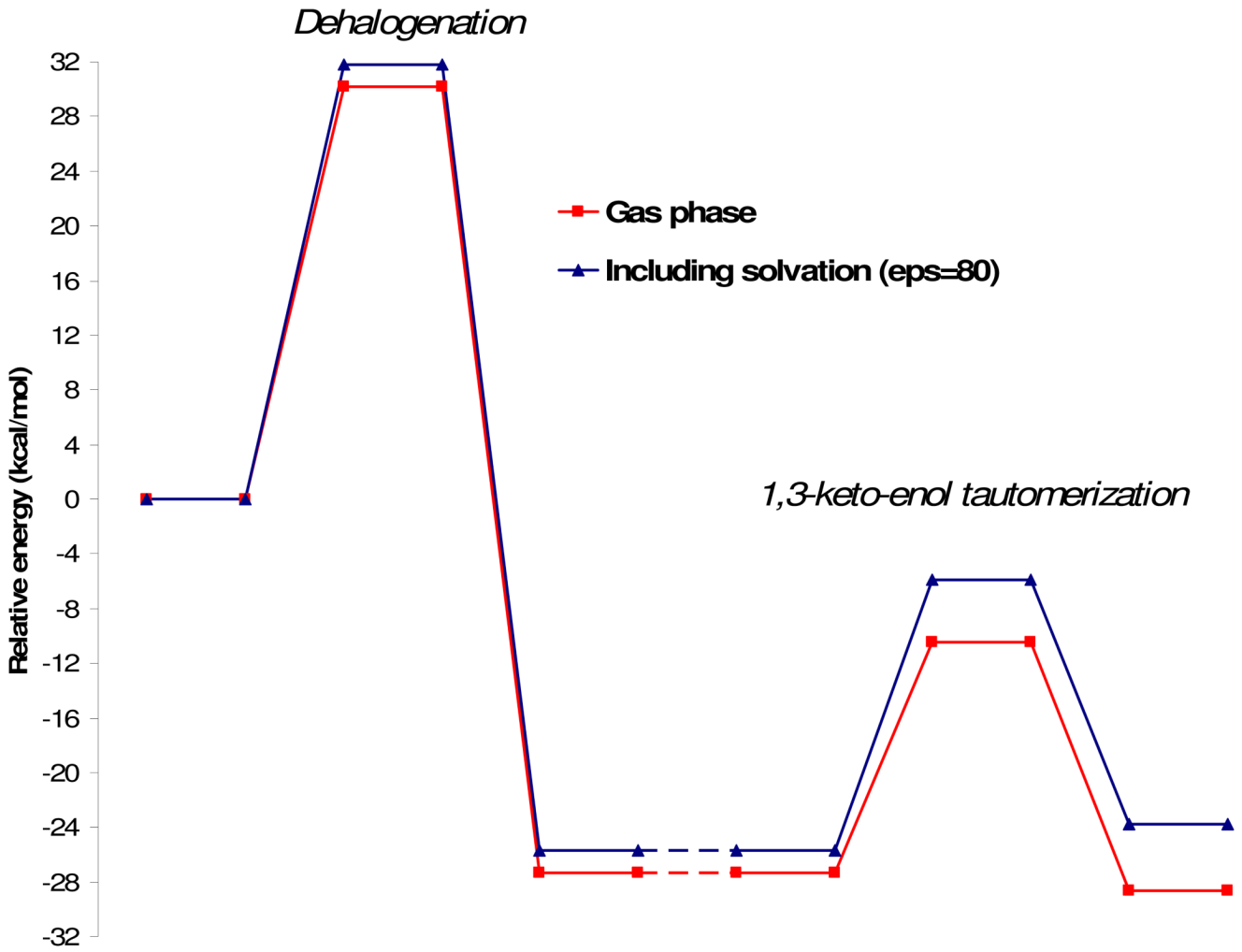

Figure 2.
Calculated potential energy curve for the uncatalyzed reaction.

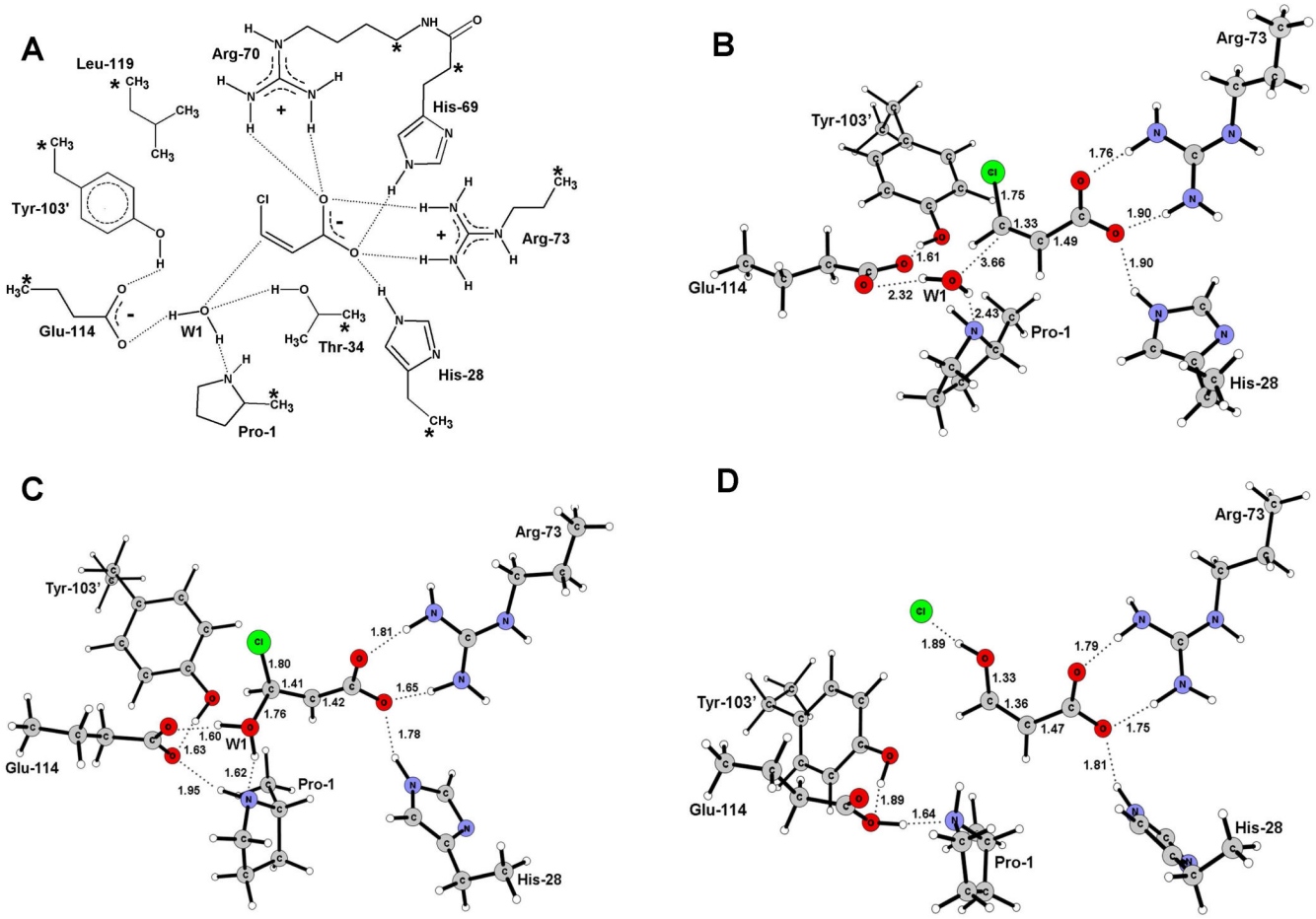

Figure 3.

Optimized geometries of the enzymatic model of cis-CaaD with a neutral Pro-1. A) Schematic drawing of the model. B) Reactant geometry. C) Transition state geometry. D) Product geometry. Optimized distances shown in Ångstrom. Stars indicate centers that are fixed to their crystallographic positions during geometry optimization, as discussed in the text. For clarity, several groups were omitted in the ball-and-stick structures (B-D).

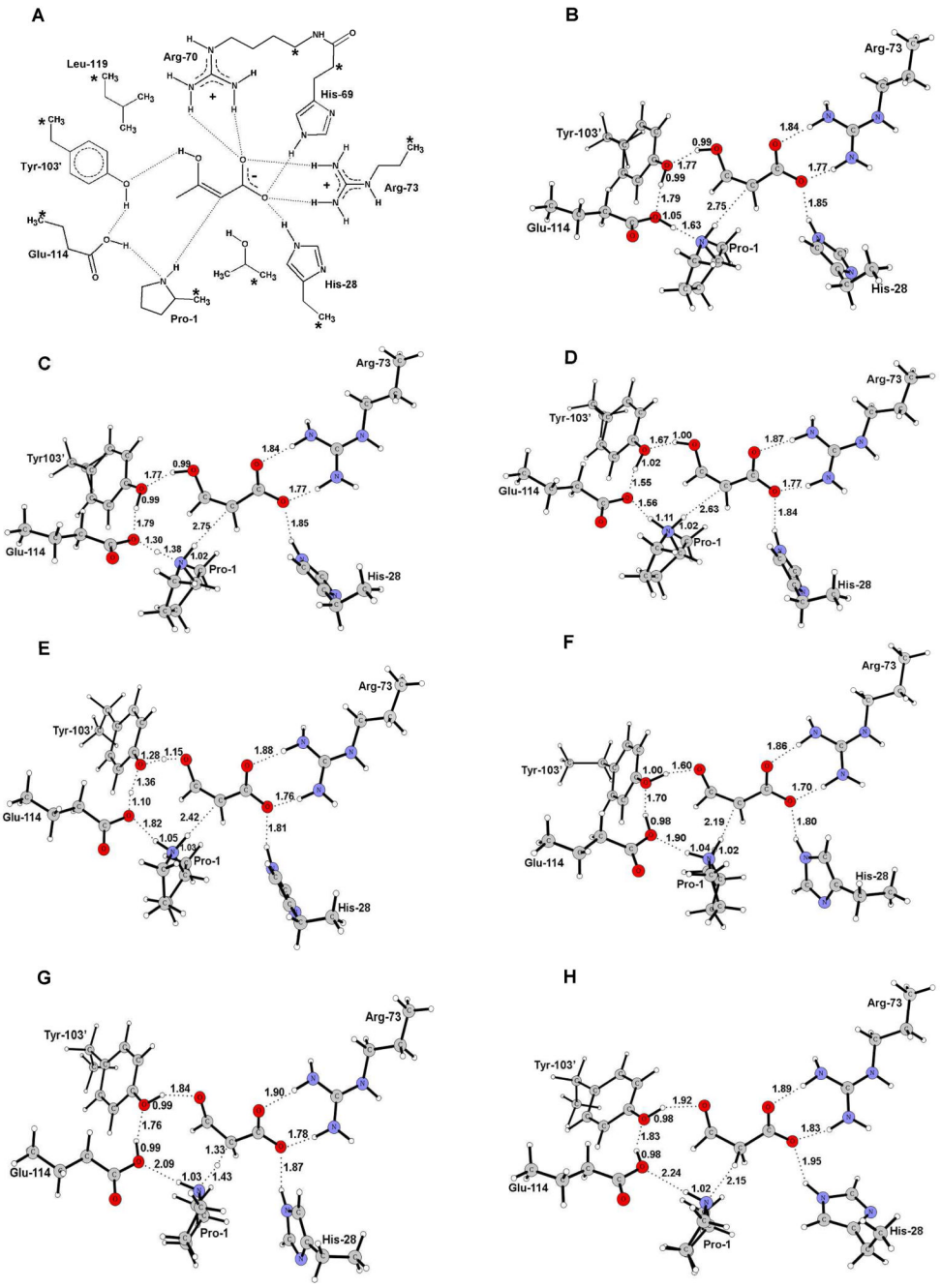

Figure 4.

Optimized stationary points for a proposed enzymatic keto-enol reaction. A) Schematic drawing of the model. B) Enol intermediate. C) TS for proton transfer from Glu-114 to Pro-1. D) Resulting intermediate with a cationic Pro-1. E) TS for the coupled proton transfers from substrate to Tyr-103' and from Tyr-103' to Glu-114. F) Resulting enolate intermediate. G) TS for proton transfer from Pro-1 to substrate. H) Final product. For clarity, several groups were omitted in the ball-and-stick structures (B-H).

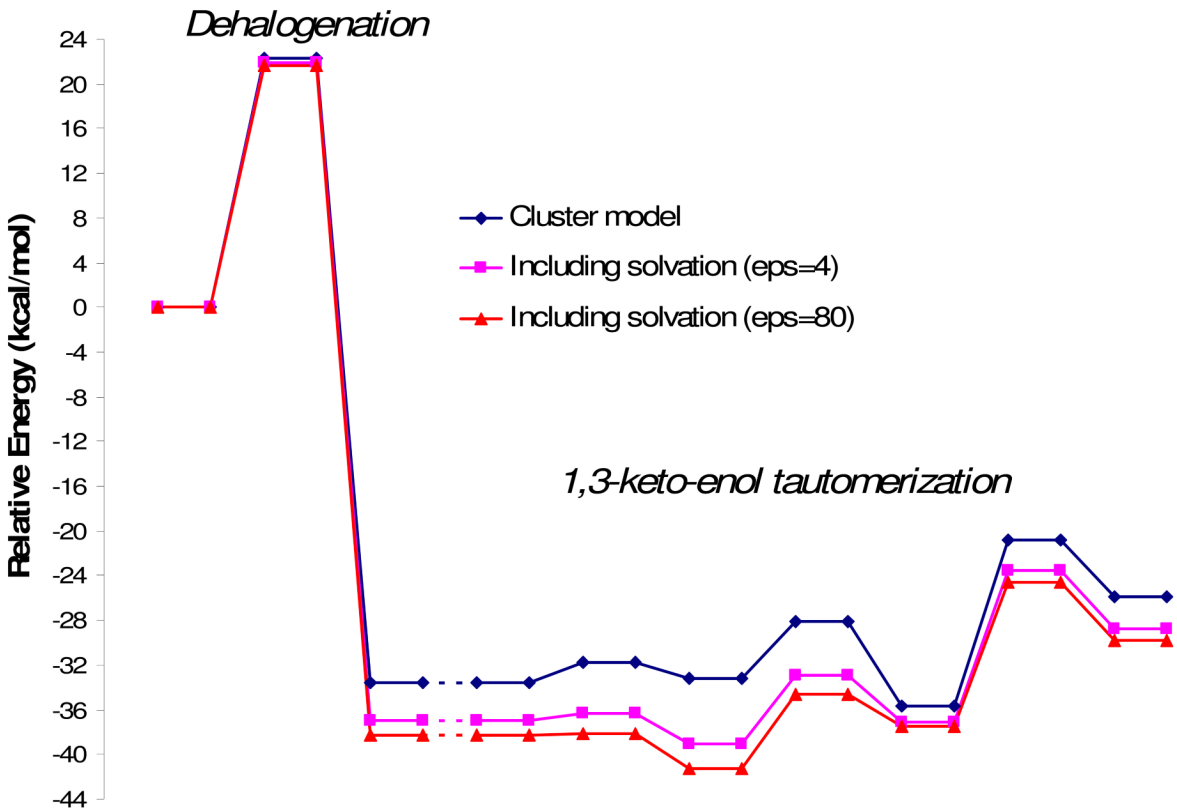

Figure 5.
Calculated potential energy curve for the cis-CaaD reaction. ε = 4 is the standard dielectric constant used to model protein surrounding and ε = 80 corresponds to water solution.

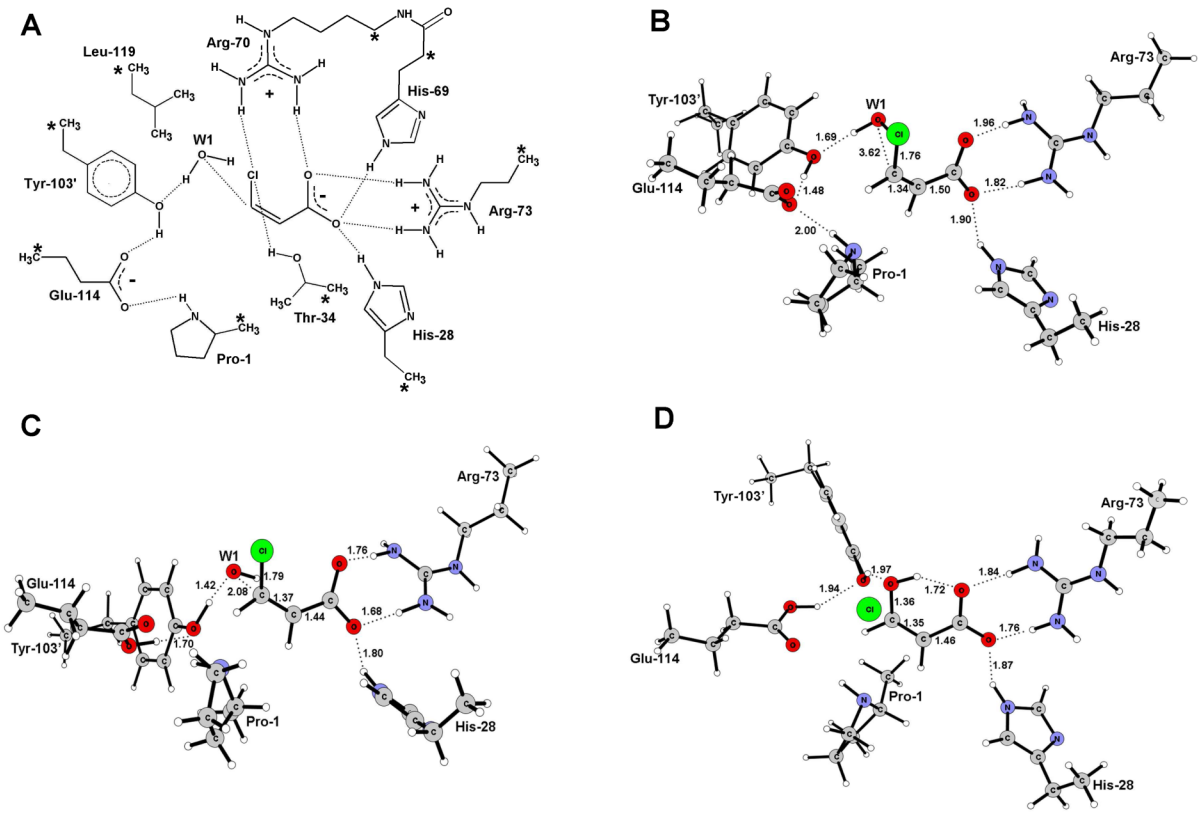

Figure 6.

Optimized geometries of the enzymatic model of cis-CaaD with a neutral Pro-1 and an alternative position of the water molecule. A) Schematic drawing of the model. B) Reactant geometry. C) Transition state geometry. D) Product geometry. Optimized distances shown in Å. Stars indicate centers that are fixed to their crystallographic positions during geometry optimization. In the ball-and-stick structures (B-D), several groups were omitted for clarity.

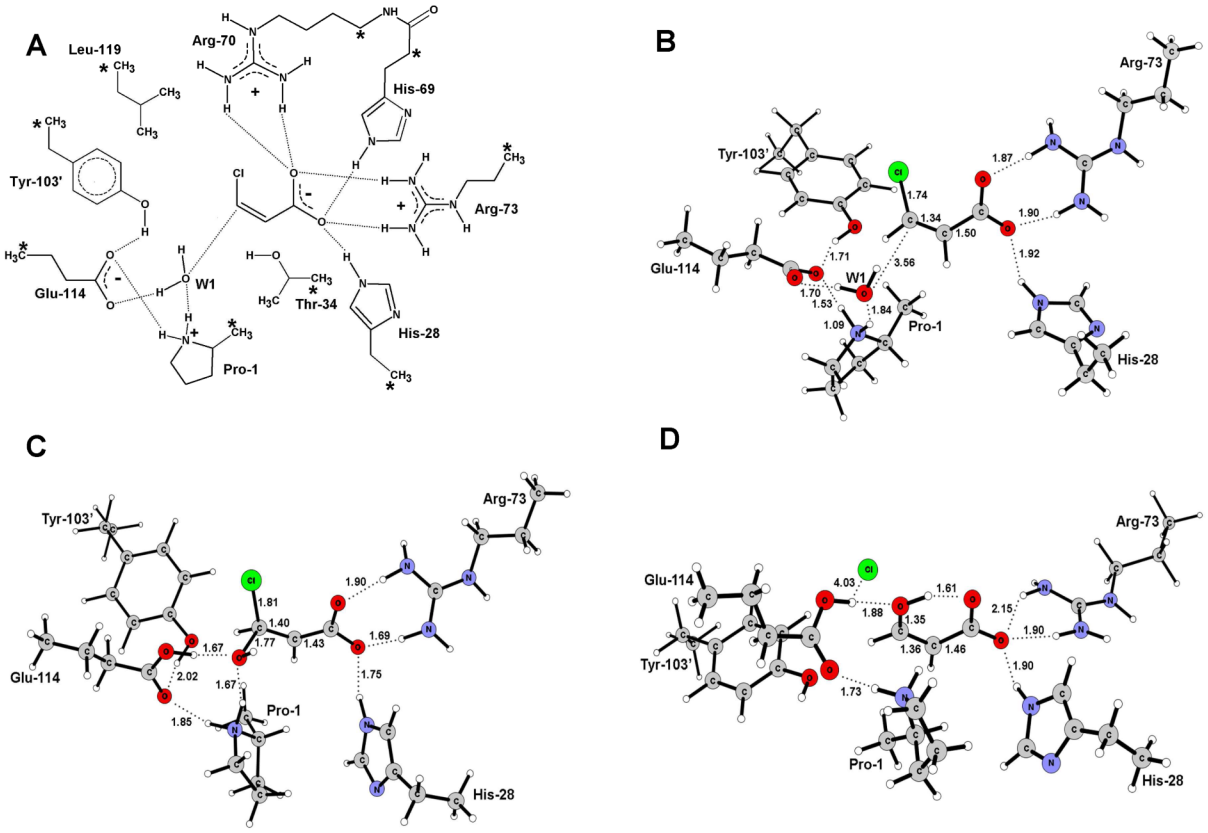

Figure 7.
Optimized geometries of the enzymatic model of cis-CaaD with a cationic Pro-1. A) Schematic drawing of the model. B) Reactant geometry. C) Transition state geometry. D) Product geometry. Optimized distances shown in Å. Stars indicate centers that are fixed to their crystallographic positions during geometry optimization. In the ball-and-stick structures (B-D), several groups were omitted for clarity.

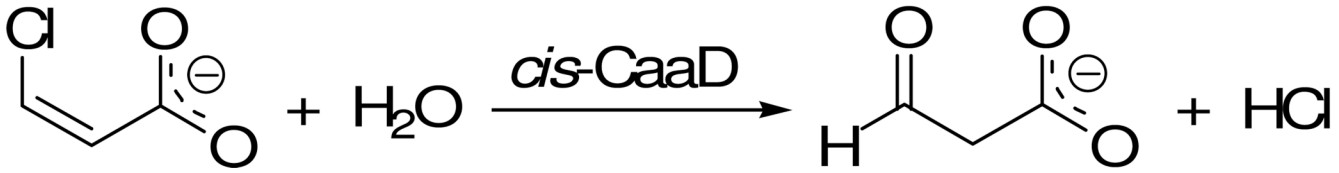

Scheme 1.
Reaction catalyzed by cis-3-chloroacrylic acid dehalogenase

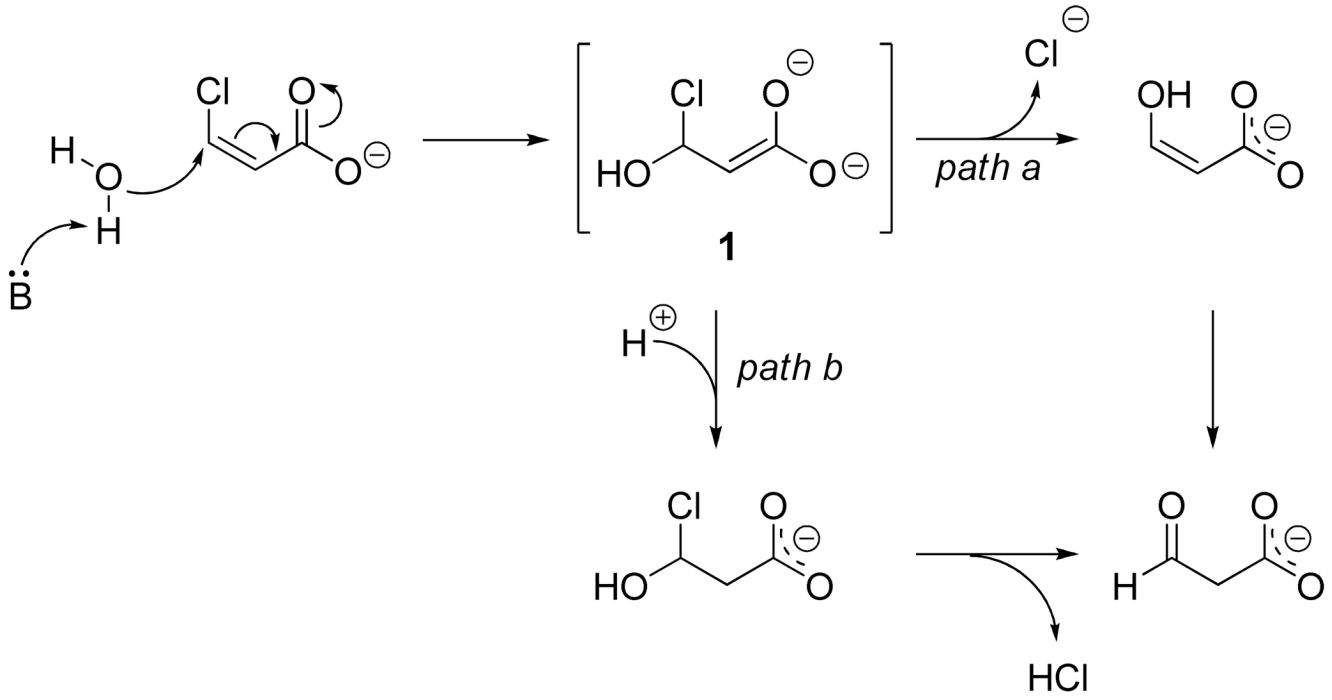

Scheme 2.
Proposed reaction mechanisms for cis-3-chloroacrylic acid dehalogenase.

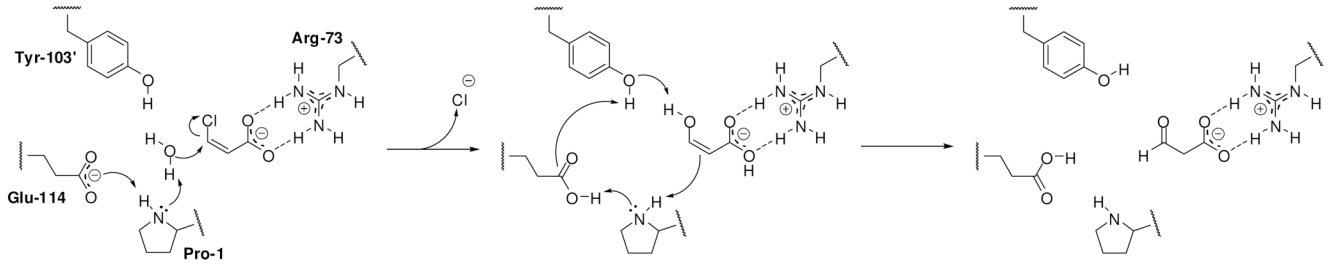

Scheme 3.
Main elements of the cis-CaaD reaction mechanism suggested from the calculations.

Table 1

Summary of calculated energies for the dehalogenation step in active site model.

	Neutral Pro-1		Alt. water binding		Cationic Pro-1	
	Barrier	**Reaction energy**	**Barrier**	**Reaction energy**	**Barrier**	**Reaction energy**
Cluster Model	22.3	−33.6	20.6	−32.4	27.6	−0.2
ε = 4	21.9	−36.9	26.4	−31.6	31.7	−3.2
ε = 80	21.7	−38.3	28.5	−31.4	33.1	−4.6

Biochemistry. Author manuscript; available in PMC 2010 October 13.